

# Mass outflow of the X-ray emission line gas in NGC 4151

S. B. Kraemer<sup>1</sup> , T. J. Turner<sup>2</sup>, D. M. Crenshaw<sup>3</sup> , H. R. Schmitt<sup>4</sup>,  
M. Revalski<sup>5</sup> and T. C. Fischer<sup>5</sup>

<sup>1</sup>Department of Physics, Institute for Astrophysics and Computational Sciences,  
The Catholic University of America, Washington, DC 20064, USA  
email: [kraemer@cua.edu](mailto:kraemer@cua.edu)

<sup>2</sup>Department of Physics, University of Maryland Baltimore County, Baltimore,  
MD 21250 U.S.A

<sup>3</sup>Department of Physics and Astronomy, Georgia State University, 25 Park Place,  
Room 631, Atlanta, GA 30303, USA

<sup>4</sup>Naval Research Laboratory, Washington, DC 20375, USA

<sup>5</sup>Space Telescope Science Institute, Baltimore, MD 21218, USA

**Abstract.** We have analyzed *Chandra*/High Energy Transmission Grating spectra of the X-ray emission line gas in the Seyfert galaxy NGC 4151. The zeroth-order spectral images show extended H- and He-like O and Ne, up to a distance  $r \sim 200$ pc from the nucleus. Using the 1st-order spectra, we measure an average line velocity  $\sim 230$  km s<sup>-1</sup>, suggesting significant outflow of X-ray gas. We generated Cloudy photoionization models to fit the 1st-order spectra; the fit required three distinct emission-line components. To estimate the total mass of ionized gas ( $M$ ) and the mass outflow rates, we applied the model parameters to fit the zeroth-order emission-line profiles of Ne IX and Ne X. We determined an  $M \approx 5.4 \times 10^5 M_{\odot}$ . Assuming the same kinematic profile as that for the [O III] gas, derived from our analysis of *Hubble Space Telescope*/Space Telescope Imaging Spectrograph spectra, the peak X-ray mass outflow rate is approximately  $1.8 M_{\odot} \text{ yr}^{-1}$ , at  $r \sim 150$ pc. The total mass and mass outflow rates are similar to those determined using [O III], implying that the X-ray gas is a major outflow component. However, unlike the optical outflows, the X-ray emitting mass outflow rate does not drop off at  $r > 100$ pc, which suggests that it may have a greater impact on the host galaxy.

**Keywords.** galaxies:active – galaxies: individual: NGC 4151 – galaxies: Seyfert – X-rays: galaxies

---

## 1. Introduction

Active galactic nuclei (AGN) are powered by the accretion of matter onto a supermassive black hole (SMBH), which generates huge amounts of radiation from a very small volume. AGN are capable of generating powerful outflows, or winds, which are believed to be critical to the structure, energetics, and evolution of AGN and their connection to their host galaxies. Specifically, the relation between bulge mass and black hole mass, the so-called  $M_{BH} - \sigma_*$  relation (Gebhardt *et al.* 2000), is thought to be regulated by AGN outflows, i.e., “AGN feedback” (Begelman 2004).

The narrow line regions (NLRs) in AGN can extend from a few parsecs to several kpc, depending on luminosity, and hence offer unique insight into the interaction of the AGN with its host galaxy. NLR-scale outflows have been studied via *Hubble Space Telescope* (*HST*)/Space Telescope Imaging Spectrograph (STIS) observations

(e.g., Fischer *et al.* 2013, 2018) and ground-based spectra, such as those obtained with the *Gemini*/Near Infrared Integral Field Spectrograph (e.g., Storchi-Bergmann *et al.* 2010; Riffel *et al.* 2013; Fischer *et al.* 2017). The NLR outflows extend to kpc scales (Fischer *et al.* 2018), where much of the nuclear star-formation occurs. Furthermore, most of the mass in these outflows is accelerated in situ, due to the radiation pressure from the AGN accelerating material in the disk of the host galaxy. Hence, the NLR-scale outflows directly reveal the interaction of the AGN with the host galaxy.

Although the NLR outflows are often massive (e.g., mass of  $\sim 10^6 M_{\odot}$ , Revalski *et al.* 2018b), and may inject large amounts of kinetic energy and momentum into the interstellar medium (ISM) of the host galaxy (e.g., Revalski *et al.* 2018a), they do not appear to be able to escape the inner kpc of the host galaxy bulge (Fischer *et al.* 2018). This calls into question the effectiveness of AGN-driven outflows in feedback. However, these results are generally derived from optical or near-IR emission line kinematics, they do not take into account the role of higher-ionization gas. For example, X-ray winds, in the form of Ultra Fast Outflows (e.g. Tombesi *et al.* 2010), appear to be able to drive large-scale molecular outflows in ULIRGs (Tombesi *et al.* 2015). Therefore, it is plausible that the X-ray gas can entrain and accelerate the optical emission-line gas.

*Chandra*/ACIS images of the nearby Seyfert galaxies NGC 4151 (Ogle *et al.* 2000) and NGC 1068 (Young *et al.* 2001) revealed extended soft X-ray emission, co-located with the [O III] emission-line gas. Bianchi *et al.* (2006) determined that this was the case for most Seyfert galaxies. *Chandra* imaging has been used to map and model the NLR X-ray emission in several Seyferts, e.g. NGC 4151 - Wang *et al.* (2011a,b,c), NGC 3393 - Maksym *et al.* (2019) and Mrk 573 - Gonzalez-Martin *et al.* (2010). By isolating bands dominated by emission-lines, e.g., Ne IX 13.7 Å, these authors were able to derive constraints on the ionization structure of the X-ray emission-line regions. In particular, Maksym *et al.* and Wang *et al.* suggest that there is evidence for shocks, indicative of the interaction of the X-ray with the ISM of the host galaxy. However, the image data, as opposed to spectra obtained with the *Chandra*/High Energy Transmission Grating (HETG), lack the spectral resolution to constrain the kinematics of the X-ray emitting gas. In contrast, Kallman *et al.* (2014) performed a detailed photoionization analysis of HETG spectra of NGC 1068 and were able to derive estimates of the total mass and mass outflow rates of the emission-line gas  $M \approx 3.7 \times 10^5 M_{\odot}$  and  $\dot{M}_{out} \sim 0.3 M_{\odot} \text{ yr}^{-1}$ , respectively. Here we summarize the results of our analysis of the 240 ksec HETG observation of NGC 4151 (Kraemer *et al.* 2020).

## 2. Observations and Analysis

We obtained a 240 ksec *Chandra*/HETG observation of NGC 4151 (OSBID 16089/19060; 2014 February). These data were split into two epochs due to constraints in the roll angle alignment to meet the observation goals, i.e., to allow us to have the cross-dispersion direction correctly oriented to observe the extended emission of NGC 4151 (see Ogle *et al.* 2000). The full, unfolded spectrum is shown in Figure 1 (left hand panel). The intrinsic continuum was heavily absorbed and in a low-flux state (Couto *et al.* 2016), which enabled the isolation of numerous emission features, such as H- and He-like lines from O, Ne, Mg, and Si, Fe K $\alpha$ , Si K $\alpha$  and various radiative recombination continua.

The emission-line morphology is revealed via the zero-th order spectra, as shown in Figure 1 (right hand panel). The continuum, both at 2.05-2.25 keV and 5.60-6.00 keV, is roughly symmetric and centered on the nucleus. The Si K $\alpha$  and Fe K $\alpha$  lines are also strongly centrally peaked, again with a slight extension to the NE. The location of the peak of the emission encompasses the innermost region of the AGN, consistent an origin in the putative torus. The lines with energies  $> 1.3$  keV, e.g., Si XIV, Si XIII, and Mg XII, are also quite compact. On the other hand, there is evidence that Mg XI is extended

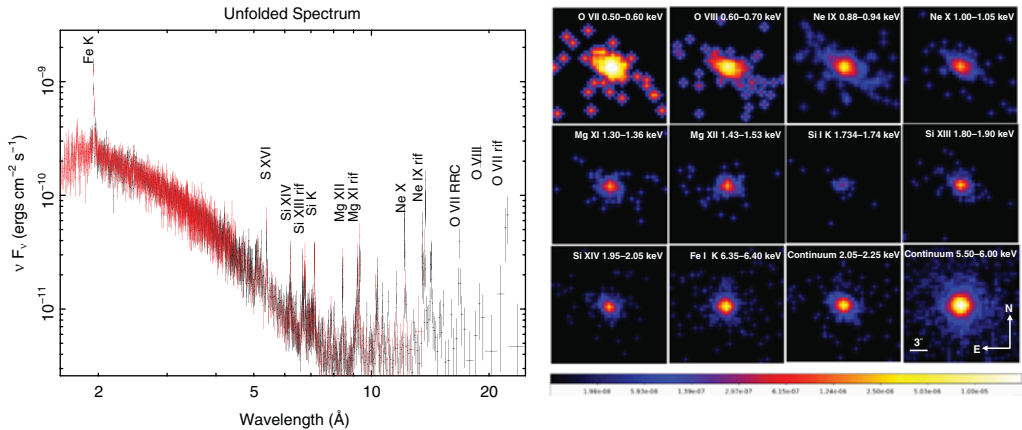


**Figure 1.** *left hand panel:* Full,  $\pm 1^{\text{st}}$  order, HETG spectrum from 1.59 Å–24.8 Å, from the summed OBSIDS. The red and black points are from the HEG and MEG, respectively. The data were binned to a minimum of 10 counts (per bin). The turn-over towards lower energies (greater wavelengths) is due to intrinsic absorption (see [Couto et al. 2016](#)). Emission at wavelengths  $> 6\text{Å}$  is emission-line dominated. *right hand panel;* Emission profiles for hydrogen and helium-like O, Ne, Mg, and Si lines, and Si  $K\alpha$  and Fe  $K\alpha$  lines, from the zeroth-order HETG spectra. Line-free regions of continuum in the ranges 2.05–2.25 keV and 5.50–6.00 keV are also shown. The images have been smoothed with a Gaussian function with kernel radius of  $1''$ , and are equally scaled for comparison in the colorbar in terms of total number of counts. The spatial scale and orientation are shown in the lower right panel.

along the NE-SW direction. Lines with energies  $\leq 1.05$  keV, i.e., Ne X, Ne IX, O VIII, and O VII, are all clearly extended along a NE-SW direction, out to a projected distance of  $>200$  pc.

To measure line fluxes, we used the combined 1st-order spectra. We fitted a Gaussian model and local continuum (using a power-law, with an un-constrained slope) for a restricted bandpass close to the line, using  $\chi^2$  statistics. The width of the bandpass used depended on the particular region, i.e. whether it was crowded or the line was isolated. The line flux and observed energy were then fitted for most lines. The average radial velocity, with upper and lower limits, is  $v_r = -230_{-370}^{+90}$  km s $^{-1}$ . Although there is evidence for a relationship between velocities and the ionization potential for optical and UV lines in some Seyfert galaxies ([Kraemer & Crenshaw 2000](#); [Kraemer et al. 2009](#)), which suggests a multi-component NLR, we found no strong evidence of such a relationship in NGC 4151 ([Kraemer et al. 2000](#)). Therefore, while the X-ray emission line gas consists of components of different ionization, there is no evidence for kinematic differences among them.

The details of the spectral fitting are given in [Kraemer et al. \(2020\)](#). In summary, we generated grids of Cloudy photoionization models ([Ferland et al. 2017](#)) over a range of values of ionization parameter,  $U$ , and column density,  $N_H$ , using the default energy resolution. We converted the Cloudy output to fittable grids using the CLOUDY-to-XSPEC interface ([Porter et al. 2006](#)). The emission features were fit via the additive emission components (ATABLES). The final ATABLE parameters,  $\log U$ ,  $\log N_H$ , were: 1.0, 22.5; 0.19, 22.5;  $-0.50$ , 23.0.

We then applied the 1st-order results to fit the extended emission, using the zeroth order HETG image. We measured the Ne X and Ne IX fluxes in a region oriented along the major axis of the optical NLR, as shown in Figure 2 (left hand panel). The emission line profiles show structure similar to that of [O III] (Figure 2, middle and right hand panels), indicating that the X-ray and optical emission-line gas have similar morphologies. Using the density law from [Crenshaw et al. \(2015\)](#), we generated photoionization models

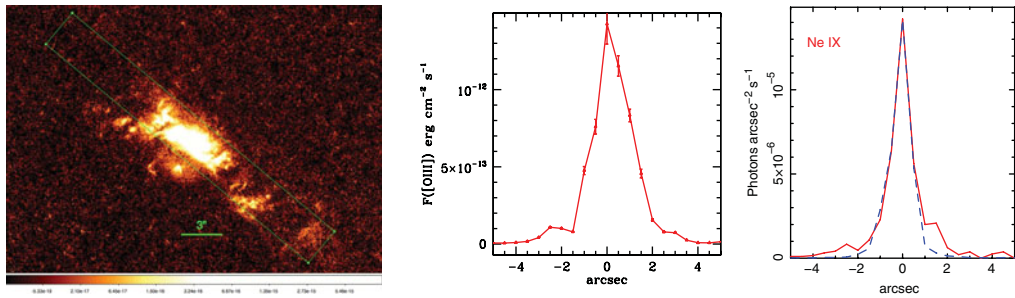


**Figure 2.** *left hand panel:* The  $0''.5 \times 3''.0$  extraction region used to obtain the Ne IX and Ne X profiles, along position angle  $140^\circ$ , superimposed upon an archival WFPC2 [O III] image of NGC 4151. North up, east to left. *middle panel:* [O III] fluxes measured within the same extraction bins; the error bars show the standard deviations which were calculated by measuring the root mean squares of fluxes in the extraction window and multiplying this number by the square root of the number of pixels in this extraction region. Positive positions are those southwest (SW) of the nucleus. *right hand panel:* Ne IX emission-line profile (in red) as a function of position. The fluxes were measured from the zeroth order HETG spectrum. The blue dashed line is the continuum; positive positions are SW of the nucleus

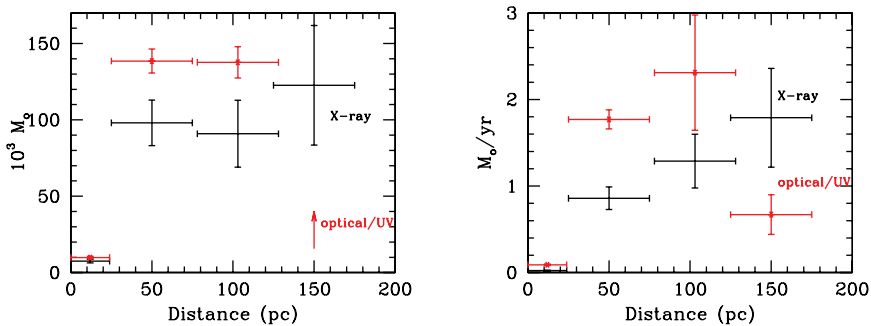


**Figure 3.** *left hand panel:* Computed  $M$  values at the same radial distances (SW and NE values summed) for the HETG analysis (black crosses), compared to those from the STIS optical/UV analysis (red asterisks), from Crenshaw *et al.* (2015) and Revalski *et al.* (2018b). The optical/UV points are summed to correspond with the HETG extraction bin sizes. Uncertainties in the optical/UV points are those from Crenshaw *et al.*, and have been added in quadrature to account for the binning. *right hand panel:* Computed values of  $\dot{M}_{out}$  as a function of distance, from the HETG analysis (black crosses), compared to those from the STIS optical/UV analysis (red asterisks). For both datasets, the  $\dot{M}_{out}$  values were computed using flux-weighted velocities within each bin from the STIS analysis. Uncertainties include both those of the mass values and the flux-weighted velocities.

for each extraction bin in order to determine  $M$  as a function of de-projected radial distance,  $r$ . In Figure 3,  $M$  and  $\dot{M}_{out}$  of the X-ray and optical gas are shown for  $r < 200$  pc. The peak X-ray mass outflow rate is  $\approx 1.8 \text{ M yr}^{-1}$ , at  $r \sim 150$  pc. While the  $M$  and  $\dot{M}_{out}$  values are similar for both components, the X-ray emitting mass outflow does not appear to diminish for  $r > 100$  pc.

### 3. Summary and Conclusions

The similarity in the mass profile, total mass, and mass outflow rates between the X-ray and optical gas suggest that the former is dynamically important in the inner nucleus of NGC 4151. Nevertheless, several open issues remain.

1) The origin of the X-ray gas is uncertain. One possibility is that it is formed via thermal expansion of the [O III] emission-line gas. Crenshaw *et al.* (2015) and Fischer *et al.* (2017) have suggested that the optical NLR gas in Seyferts originates in the disk of the host galaxy, and is ionized and accelerated, by the AGN, in situ. Also, the [O III] knots do not appear to travel far from their point of origin (Fischer *et al.* 2017). An intriguing possibility is that the optical outflows evolve into X-ray emitting winds (Trindade Falcão *et al.*, in preparation).

2) A major limit to this analysis (see also Gonzalez-Martin *et al.* 2010) is the lack of spatially resolved X-ray kinematics. However, highly ionized optical emission lines, e.g. [Fe X]  $\lambda$ 6374, [Fe IX]  $\lambda$ 7892, and [Fe XIV]  $\lambda$ 5303, are formed in the same range of ionization as the X-ray emission-line gas. Hence, they are potential “footprints” of X-ray winds. These lines can be mapped with *HST*/STIS (e.g., Kraemer *et al.* 2000) and offer the possibility of tracking the X-ray wind kinematics.

## References

- Begelman, M. C. 2004, in Carnegie Observatories Astrophysics Series, Vol. 1, Coevolution of Black Holes and Galaxies, from the Carnegie Observatories Centennial Symposia, ed. L. Ho, 374–390
- Bianchi, S., Guainazzi, M., & Chiaberge, M. 2006, *A&A*, 448, 499
- Couto, J., Kraemer, S., Turner, T., *et al.* 2016, *ApJ*, 833, 191
- Crenshaw, D. M., Fischer, T. C., Kraemer, S. B., *et al.* 2015, *ApJ*, 799, 83
- Ferland, G. J., Chatzikos, M., Guzman, F., *et al.* 2017, *Rev.Mexicana AyA*, 53, 385
- Fischer, T. C., Crenshaw, D. M., Kraemer, S. B., *et al.* 2013, *ApJS*, 209, 1
- Fischer, T. C., Machuca, C., Diniz, M. R., *et al.* 2017, *ApJ*, 834, 30
- Fischer, T. C., Kraemer, S. B., Schmitt, H. R., *et al.* 2018, *ApJ*, 856, 102
- Gebhardt, K., Bender, R., Bower, G., *et al.* 2000, *ApJ*, 539, L13
- Gonzalez-Martin, O., Acosta-Pulido, J. A., Perez Garcia, A. M., *et al.* 2010, *ApJ*, 723, 1748
- Kallman, T. R., Evans, D. A., Marshall, H., *et al.* 2014, *ApJ*, 780, 121
- Kraemer, S. B. & Crenshaw, D. M. 2000, *ApJ*, 532, 256
- Kraemer, S. B., Crenshaw, D. M., Hutchings, J. B., *et al.* 2000, *ApJ*, 531, 278
- Kraemer, S. B., Trippe, M. L., Crenshaw, D. M., *et al.* 2009, *ApJ*, 698, 106
- Kraemer, S. B., Turner, T. J., Couto, J. D., *et al.* 2020, *MNRAS*, 493, 3893
- Maksym, W. P., Fabbiano, G., Elvis, M., *et al.* 2019, *ApJ*, 872, 94
- Ogle, P. M., Marshall, H. L., Lee, J. C., *et al.* 2000, *ApJ*, 545, L81
- Porter, R. L., Ferland, G. J., Kraemer, S. B., *et al.* 2006, *PASP*, 118, 920
- Revalski, M., Crenshaw, D. M., Kraemer, S. B., *et al.* 2018a, *ApJ*, 856, 46
- Revalski, M., Dashtamirova, D., Crenshaw, D. M., *et al.* 2018b, *ApJ*, 867, 88
- Riffel, R. A., Storchi-Bergmann, T., & Winge, C. 2013, *MNRAS*, 430, 2249
- Storchi-Bergmann, T., Lopes, R. D. S., McGregor, P. J., *et al.* 2010, *MNRAS*, 402, 819
- Tombesi, F., Cappi, M., Reeves, J. N., *et al.* 2010, *A&A*, 521, A57
- Tombesi, F., Melédez, M., Veilleux, S., *et al.* 2015, *Nature*, 519, 436
- Wang, J., Fabbiano, G., Elvis, M., *et al.* 2011a, *ApJ*, 736, 62
- Wang, J., Fabbiano, G., Risaliti, G., *et al.* 2011b, *ApJ*, 729, 75
- Wang, J., Fabbiano, G., Elvis, M., *et al.* 2011c, *ApJ*, 742, 23
- Young, A. J., Wilson, A. S., & Shopbell, P. L. 2001, *ApJ*, 556, 6